Check for updates

Decadal mapping of flood inundation and damage assessment in the confluence region of Rivers Niger and Benue using multi-sensor data and Google Earth Engine

Caleb Odiji [a,*], Godstime James[a], Ademuyiwa Oyewumi[a], Shomboro Karau[a], Belinda Odia[a], Halima Idris[a,b], Olaide Aderoju[a] and Abubakar Taminu[a]

[a] Department of Strategic Space Application, National Space Research and Development Agency, Airport Road, P.M.B. 437, Abuja, Nigeria
[b] Department of Geography, Nigerian Defence Academy, Kaduna, Nigeria
*Corresponding author. E-mail: odijic@yahoo.com

CO, 0000-0003-2379-5603

ABSTRACT

Climate change has made weather patterns more extreme, causing floods in Nigeria. Flooding is the most frequent and serious natural hazard in the confluence region of Rivers Niger and Benue, impacting lives, agriculture, and socio-economic activities significantly. Advancements in satellite technology and computational capabilities have enhanced rapid information about flood extent for monitoring, mitigation, and planning. However, there is a dearth of information based on time series analysis of flood inundation and monitoring in the confluence region. In this study, Sentinel-1 Synthetic Aperture Radar, Sentinel-2, and Landsat-7 and Landsat-8 data were used to extract flood inundation for 10 years (2012–2022) in the confluence region of Rivers Niger and Benue. Flood extent/surface waterbodies were extracted using the Google Earth Engine platform, modified normalized difference water index, and normalized difference water index methods. The findings revealed that within 10 years, four significant flooding incidents occurred in 2012, 2018, 2020, and 2022, inundating 60.57, 48.24, 39.98, and 84.39 km^2 of the area, respectively. The study underscores the need for the establishment of a decision support system for monitoring flood inundation and providing decision-makers necessary information for flood disaster preparedness, mitigation, and adaptation.

Key words: Benue, confluence region, inundation, Niger, Synthetic Aperture Radar

HIGHLIGHTS

- Mapping and monitoring flood inundation were done by intersecting Sentinel-1 Synthetic Aperture Radar, Landsat-7 and Landsat-8, and Sentinel-2 datasets.
- Surface water was extracted using the modified normalized difference vegetation index and Google Earth Engine.
- These data are used to conduct time series flood inundation mapping, which is lacking in most studies.

GRAPHICAL ABSTRACT
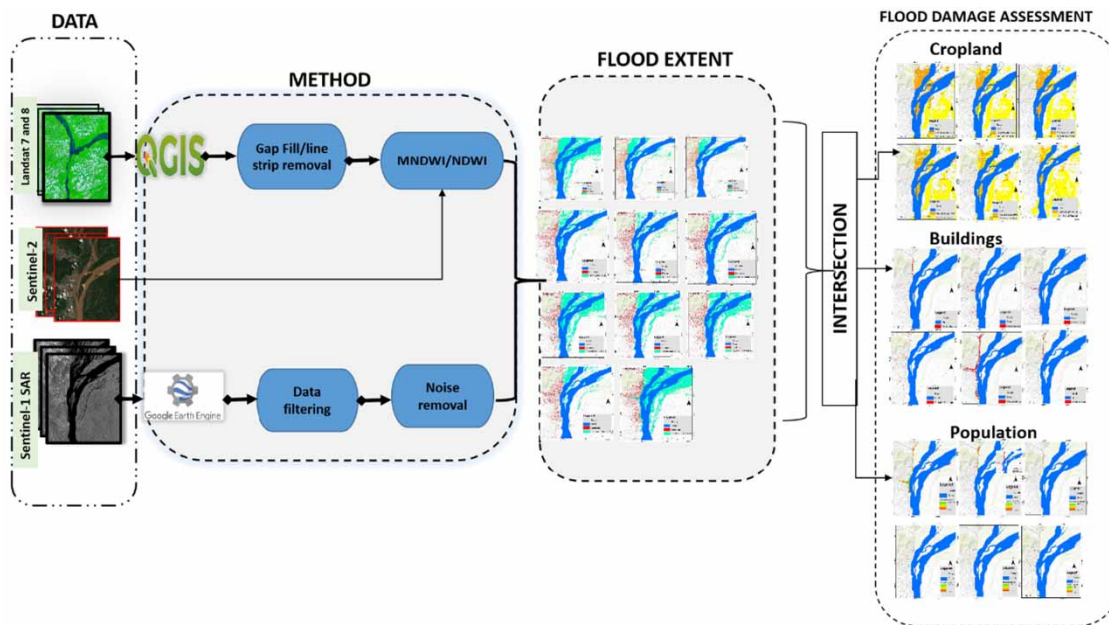
1. INTRODUCTION

Flooding is one of the most prevalent and devastating natural disasters that disrupt people's lives and livelihoods worldwide (Phy *et al.* 2022). Floods frequently cause irreparable damage and misery, particularly in low-income nations with poorly established infrastructure systems such as drainage and flood protection. Flood inundation depths of more than 0.15 m directly affect around 1.47 billion people or 19% of the world's population. Furthermore, for more than half of this vulnerable population, flooding might be significantly worse, possibly life-threatening, especially for children and people with disabilities (Rentschler & Salhab 2020).

As the frequency and intensity of flood occurrences have increased due to climate change, global concerns about reducing casualties and other economic disruptions have grown (Kuldeep *et al.* 2016). The intensity and frequency of flood inundation are required for assessing society's exposure, infrastructure loss, economic loss, crop damage, and urban flooding. For example, there were 3,564 flood disasters between 1996 and 2013, indicating that floods are far more common than drought (1,343) and storms (1,585) combined (United Nations Disaster Risk Reduction Preparedness & Asian Disaster Preparedness Center 2019). Floods occur in almost every part of the world with different intensities and effects. The period from 2009 to 2018 witnessed an average of 149 floods per year worldwide, leading to substantial losses across various sectors such as live-stock, crops, and property; the total economic impact of these floods amounted to over 400 billion US dollars (Centre for Research on the Epidemiology of Disasters 2020). In 2021, Asia experienced more than 100 natural hazard events, with floods and storms comprising 80% of the total. This resulted in about 4,000 fatalities, with flooding responsible for roughly 80% of them. These hazards directly impacted 48.3 million individuals, producing a total economic loss of 35.6 billion US dollars. Flooding caused the highest economic losses in China (18.4 billion US dollars), followed by India (3.2 billion US dollars), Japan (2 billion US dollars), and Thailand (0.6 billion US dollars) (World Meteorological Organization 2022).

The summer of 2005 witnessed the devastating flooding brought by Hurricane Katrina, which caused more than 108 billion US dollars in damages, constituting the costliest natural disaster in US history (Diaz *et al.* 2020). Africa, which is one of the poorest continents in the world (in terms of GDP growth and income), has experienced an increase in flood disasters in recent times (Suhr & Steinert 2022). For instance, one of the biggest flooding disasters on record struck the West and Central African regions in 2022, affecting nearly 8.5 million people across 20 countries. Heavy rains and floods have claimed 1,567 lives, injured 4,401 people, displaced 3.2 million people, and destroyed 517,000 homes across 18 nations. Nigeria, Chad, and the Democratic Republic of the Congo have been the most badly affected, with 4.5 million, 1.5 million, and 946,000 people affected, respectively. Flooding has destroyed 1.6 million hectares of agriculture, ruining harvests and jeopardizing residents'

lives (OCHA 2022b). Therefore, flood inundation mapping is critical for risk assessment/forecast improvement (Nghia *et al.* 2022), planning (Dinh *et al.* 2019), and understanding flood regimes (Rangari *et al.* 2019).

The confluence region of the Niger and Benue rivers is located in one of the most flood-prone areas in Nigeria, characterized by flat terrain and floodplains. Flooding in this region is almost a yearly occurrence that stems mainly from torrential rainfalls and the occasional release of water from the Lagdo Dam in Cameroon. Lokoja, the capital city of Kogi State, and other communities along the confluence region of the rivers are susceptible to floods after torrential rainfalls. Retrospectively, severe floods have been recorded in 2012, 2018, 2020, and 2022, resulting in the disruption of economic and social activities. The most disastrous and destructive flood event ever recorded occurred in 2012 (Aderoju *et al.* 2014). However, the recent 2022 flood has been reported to be worse than the 2012 flood, making it the worst to ever occur in this region.

Space technology and other advancements in remote sensing (RS) have enabled a diverse range of satellite data applications. Data from RS provide multi-resolution satellite data for flood inundation mapping and flood risk zone identification, which are essential in developing any flood management strategy (Sahoo & Sreeja 2017) and can be used to map flood extent in near real-time (Cohen *et al.* 2019). RS offers a synoptic view of flood areas, eliminating the need for fieldwork, which is time-consuming and labor-intensive (Güvel *et al.* 2022). With optical sensors, both temporary and permanent waterbodies can be easily distinguished from other land covers due to their spectral behavior in the visible and infrared spectra (Ji *et al.* 2009). However, optical sensor data are susceptible to inherent problems such as cloud cover, haze, and line strips (Khan *et al.* 2011). As a result, several researchers emphasize the significance of synthetic Aperture Radar (SAR) data for flood studies. SAR bands enable imagery to be obtained in all weather conditions. Sentinel-1 data have been widely used to provide a timely assessment of flood disasters (Pandey *et al.* 2022).

Google Earth Engine (GEE) is a powerful web platform for the cloud-based processing of large-scale RS data. GEE provides a cloud computing platform for storing and analyzing massive datasets up to petabytes. GEE provides a variety of constantly updated datasets that can be accessed directly within the code editor (Kumar & Mutanga 2018).

Numerous studies have been conducted on flood extent and damage assessment based on SAR and GEE. Pandey *et al.* (2022) conducted a large-scale flood mapping and impact assessment in the Ganga–Brahmaputra Basin using SAR data in GEE. Nghia *et al.* (2022) applied GEE and sentinel-1 SAR data for mapping and monitoring floods in the downstream provinces of the Mekong River. Vekaria *et al.* (2022) undertook flood mapping in the Brahmaputra River, Assam in India using multi-temporal Sentinel-1 SAR images. Other studies conducted on SAR and GEE include Tiwari *et al.* (2020), Kumar *et al.* (2022), Risling (2022), Suab *et al.* (2022), and Wang *et al.* (2022). Research on mapping flood extent and damage assessment based on multi-sensor data has been carried out by Huang *et al.* (2014) and Anusha & Bharathi (2020). Few studies have looked at the confluence region of Rivers Niger and Benue (Aderoju *et al.* 2014; Ebinne & Apeh 2019; Emmanuel & Eyoh 2017; Jimoh & Salami 2020; Adedeji *et al.* 2021). However, there is a lack of information on mapping and monitoring of flood inundation dynamics and damage assessment in the confluence region of Rivers Niger and Benue using multi-temporal sensors data and GEE on a time series basis.

Floods are becoming more frequent due to climate change, with disastrous consequences for the world's population, cropland, and environment. Flood monitoring and assessment provide information essential to track floods and offer illuminating insight into how flood hazard poses different levels of risk and estimate impacts (Güvel *et al.* 2022). Therefore, this study aims to conduct a decadal mapping of flood inundation and damage assessment in the confluence region of Rivers Niger and Benue by using Landsat, Sentinel-1 SAR, Sentinel-2, and GEE. The objectives of this study are (1) to map inundation extent from 2012 to 2022, (2) to map inundation frequency, and (3) to assess the impacts of the floods on cropland, buildings, and population. The outcome of this study is pertinent for effective flood risk management and the development of mitigation measures.

2. DATA AND METHODS

2.1. Study area

The confluence region of the two major rivers in Nigeria, River Niger and River Benue, lies between latitude 7° 45′ N to latitude 8° 12′ N and longitude 6° 39′ E to longitude 7° 00′ E. Rivers Niger and Benue are two of West Africa's largest rivers. The two rivers connect in Lokoja, the capital city of Kogi State, forming a Y-shaped structure and draining southward into the Atlantic Ocean. While the color of the Niger River is brownish, that of the Benue River is pale green. The rivers are heavily used for fishing. The area has two major seasons: the dry season and the wet season. The wet season spans from March to

October or November, while the dry season spans from November to March, with annual rainfall ranging between 1,016 and 1,524 mm and an average annual temperature of 27 °C. The study area covers 236.67 km^2, with an elevation that ranges between 45 and 400 m above sea level (Figure 1).
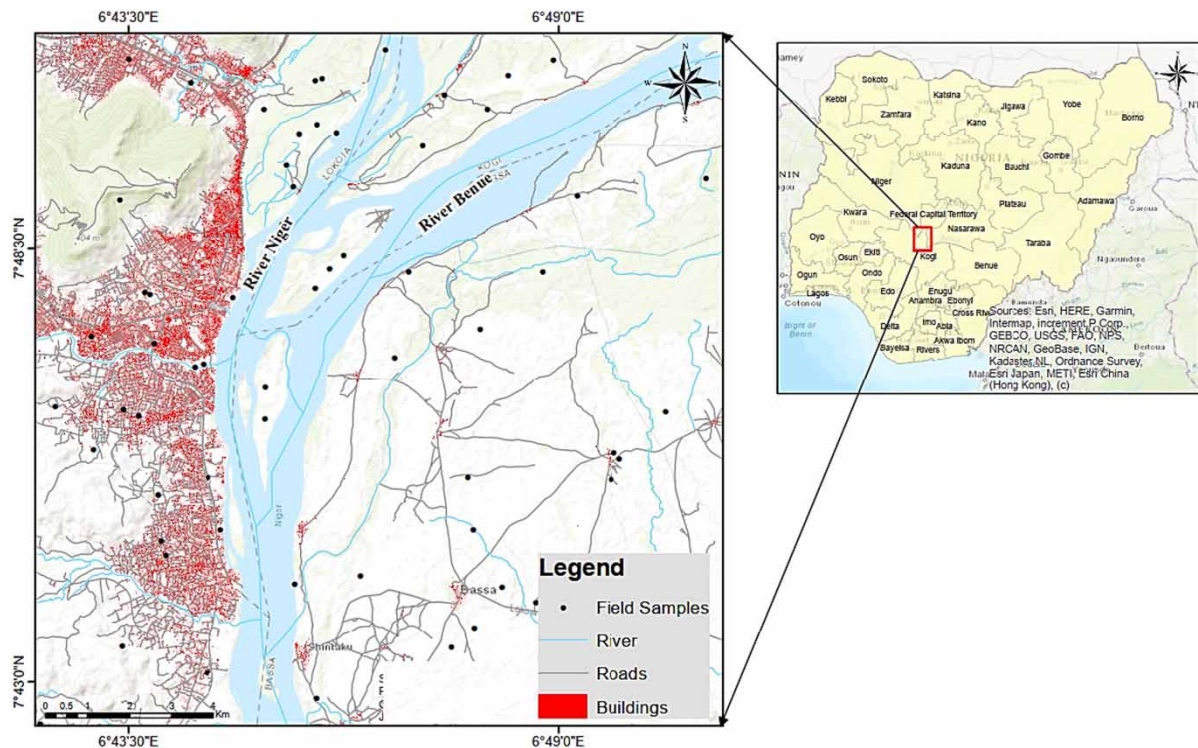
2.2. Data acquisition

The Sentinel-1 mission collects data from a C-band SAR instrument measuring vertically transmitted vertically received (VV)/vertically transmitted horizontally received (VH) dual-polarization in the interferometric wide (IW) swath mode at a frequency of 5.405 GHz. The revisit frequency of Sentinel-1 data is 12 days with one satellite and 6 days with two satellites.

The Level 1 Terrain corrected (L1T) product acquired by Operational Land Imager/Thermal Infrared Sensor (OLI/TIRS) instrument on board Landsat-8, featuring a 30-m resolution and corresponding to paths/rows of 189/55, was obtained from the United States Geological Survey for Earth Resources Observation and Science (USGS-EROS) via https://earthexplorer.usgs.gov/. The Landsat-7 images were acquired between 4th and 9th October, in both 2012 and 2013, with line strip and marginal cloud cover. Landsat-8 OLI was acquired on 4 October 2014.

To assess the impact of flood, the population per 100×100 m grid cell for the year 2020 was acquired from WorldPop Global Project Population Data via https://www.worldpop.org/. Roads, building footprints, and boundary shapes were downloaded from Open Street Map (OSM) via https://www.openstreetmap.org/. Cropland and water bodies were acquired from the global land cover map for 2020 at 10 m resolution based on Sentinel-2 data via https://cds.climate.copernicus.eu/#!/home (Table 1).

2.3. Methodology

The flowchart in Figure 2 illustrates the method adopted in this study for mapping flood inundation and damage. The extent of floods in the initial 3 years (2012, 2013, and 2014) was derived from Landsat images and combined with Sentinel-1 SAR images that had become available in 2015.

Figure 1 | Study area.

Table 1 | Data used and their specifications

Data	Acquisition date	Characteristics	Sources
Sentinel-1 SAR	20 September 2015 26 September 2016 21 September 2017 28 September 2018 23 September 2019 29 September 2020 24 September 2021 09 October 2022	Spatial resolution: 10 m Swath: 250 km Revisit period: 12 days Polarization: VV Pass direction: descending	Google Earth Engine https://earthengine.google.com/
Landsat-7 ETM+ and Landsat-8 OLI	04 October 2012 09 October 2013 04 October 2014	Spatial resolution: 30 m Revisit period: 16 days	https://earthexplorer.usgs.gov/.
Sentinel-2	20 September 2022 04 October 2022	Spatial resolution: 10 m	https://www.sentinel-hub.com/
World Pop	21 September 2022	Cell size: 100×100 m	https://www.worldpop.org/.
Building footprints, roads, and boundary shapefile	14 September 2022	Vector layers	https://www.openstreetmap.org/
SPOT-5	06 October 2012 15 October 2013	Spatial resolution: 5 m	https://eos.com/find-satellite/kompsat-3-3a/

### 2.3.1. Processing Sentinel-1 SAR data in GEE

Sentinel-1 SAR is a dataset with high-resolution imaging, allowing for large-scale geographic analysis. This dataset was used to map flooded areas in the confluence region. Sentinel-1 SAR VV polarization and IW swath acquisition mode were exploited to delineate the flood extent from 2015 to 2022. This was implemented by using the United Nation's Space-based Information for Disaster Management and Emergency Response (UN-SPIDER) recommended practice on flood mapping and damage assessment using Sentinel-1 SAR data in GEE. The recommended practice is an automated workflow system enabled by 609 lines of Java code or script inputted in GEE (https://code.earthengine.google.com/f5c2f984c053c8ea574bfcd4040d084e).

The code is optimized to map flood extent and damage assessment in several steps. Step 1 involves delineation of the area of interest. Step 2 involves data filtering: this entails setting the start and end dates of a period before and after the flood event. Images before the flood event that ranged from 1 to 15 September for the various years and images during the flood event that ranged from 20 September to 5 October of each year were filtered. The polarization was set to VV, and the pass direction was set to ascending mode. VV was used because of its performance in monitoring open water areas (Tiwari *et al.* 2020; Nghia *et al.* 2022). Step 3 involves thermal noise removal, application of a speckle filter to reduce noise pixel, and conversion of the backscatter coefficient into decibels. The radiometric conversion from a linear scale to a dB scale was conducted using the following expression:

$$\sigma^0 \mathrm{dB} = 10 \cdot \log_{10}^{\sigma^0} \tag{1}$$

where σ^0 is the backscattering image in dB and σ^0 is the sigma-nought image.

The amount of backscatter signals returned to the sensor is determined by the structure of the feature or object. The amount of backscatter signals returned to the sensor can also vary depending on polarization; for example, VH polarization has higher volume scattering returns, whereas the VV channel has higher specular scattering returns. Step 4 involves refining the flood extent layer and performing a change detection analysis. Step 5 involves importation, visualization, and flood extent calculation in ArcGIS pro-2.8. Step 6 is the intersection of population, cropland, building footprints, and road layers with the flooded extent for damage assessment (Vanama *et al.* 2020; Suab *et al.* 2022; Wang *et al.* 2022).
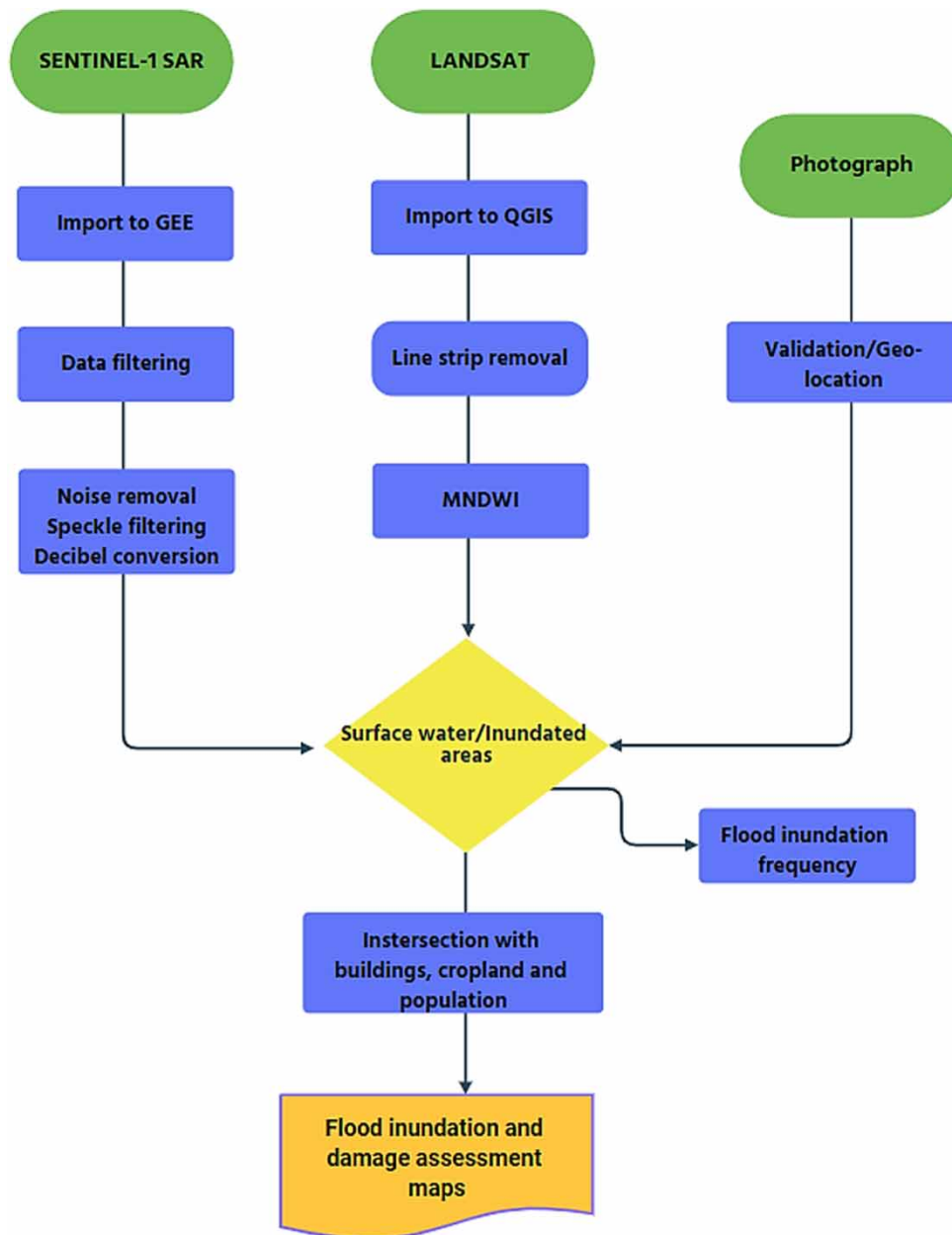
Figure 2 | Methodology flowchart.

2.3.2. Damage assessment

The effects of the floods were estimated by overlaying the maximum inundation extent on cropland, population, and building footprints. The study area is prominent for maize production in the plain by small-scale farmers. In fact, the state is among the top 10 producers of maize in Nigeria. The study estimated the potential monetary implications of the floods on maize for each year by determining the average yield per ton per hectare and multiplying by the cost per metric ton per year. The average maize yield in Nigeria reached 2 tons per hectare, remaining almost constant from previous years. The cost per metric ton varied between the years, which formed the basis for the monetary evaluation. Data for the average yield and cost metric ton were also obtained (PricewaterhouseCoopers 2021; International Institute of Tropical Agriculture IITA 2011; Nigeria 2021; Nigeria Commodity Exchange 2021). The limitations of this valuation method are the complexity of gathering, classifying, and performing estimation, which is further complicated by a lack of uniformity and variations in input quality. When

inputs are owned by the farm or when information on values or unit prices is unavailable, the use of market pricing to impute expenses may be hindered by the absence of well-functioning marketplaces for these inputs.

The flood inundation extent was also intersected with buildings and population data. The affected buildings and population were estimated using ArcGIS Pro's Select by Location and Zonal Statistics tools.

2.3.3. Water features delineation using the modified normalized difference water index (MNDWI) and normalized difference water index (NDWI)

The Landsat images of 2012, 2013, and 2014 were fraught with line strips. The line strips were removed using the Fill nodata tool in QGIS. Afterward, the MNDWI was applied to all of the Landsat images to mask out flooded areas. The MNDWI was proposed by Xu (2006) to correct this problem by suppressing land features while enhancing water features. Because of its effectiveness in decreasing and even eliminating built-up land noise, the MNDWI is more suitable for augmenting and extracting water information for a water region with a background dominated by built-up land areas. The MNDWI values for Landsat-7 and Landsat-8 were calculated using Equation (2), and the NDWI was used to calculate the water content in Sentinel-2 using Equation (3):

$$MNDWI = \frac{Green \ - \ SWIR}{Green \ + \ SWIR} \tag{2}$$

$$NDWI = \frac{Green \ - \ SWIR}{Green \ + \ SWIR} \tag{3}$$

For Landsat-7 data, MNDWI = (Band 2 − Band 5)/(Band 2 + Band 5). For Landsat-8 data, MNDWI = (Band 3 − Band 6)/(Band 3 + Band 6). For the Sentinel-2 spectral imagery, the two bands used are Bands 3 and 8. Band 3 is a green band, and Band 8 is the near-infrared band. In general, water bodies have NDWI values larger than 0.5. The threshold value is determined by analyzing data from a variety of sources, including histogram shape, entropy, comparable characteristics, geographic correlation, and grayscale. This study applied Otsu's approach (Otsu 1979) for the characterization of the grayscale diagram (Figure 3). In this study, a threshold value of 0.35–0.5 is considered ideal to achieve some level of separability in detection of water areas from non-water areas (Acharya et al. 2018; Buma et al. 2018; Mondejar & Tongco 2019).

2.3.4. Inundation frequency

Inundation frequency refers to the frequency and temporal behavior with which water returns from one year to the next (Pekel et al. 2016). Eleven maps of maximum annual inundation extent were created covering 10 years from 2012 to 2022. The inundation frequency was calculated based on the number of years an area experienced flooding at least once
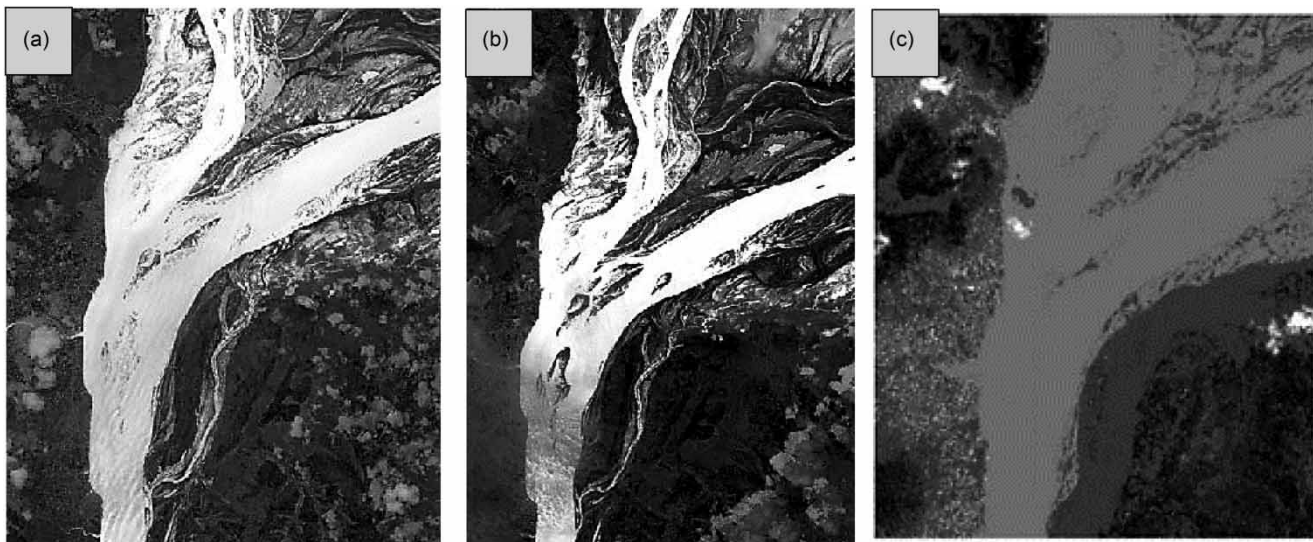
Figure 3 | Surface water detection: (a) Landsat-7 2012, (b) Landsat-8 2013, and (c) Sentinel-2 2022.

in one image within a year. The annual inundation maps were superimposed (summed) into a single-layer product, showing the frequency distribution of inundation over 10 years (Thito *et al.* 2016).

2.3.5. Validation and performance evaluation

Validation of the 2022 flood extent was based on field surveys and photographs taken from the field and online sources. The photographs were geolocated with Sentinel-2 images of the flood extent using the GPS coordinates in the photographs' metadata (Tripathy & Malladi 2022).

The open surface water bodies extracted from the different methods and sensors were validated by comparing them against reference images (Spot 5 and Sentinel-2). The extracted water bodies were reclassified as water and non-water bodies. Additionally, pixel comparison was done by overlaying 100 stratified randomly generated training sample points on the reference images and the samples, maintaining an even proportion between water and non-water areas (Zhou *et al.* 2017). A confusion matrix indicating true positive (TP), true negative (TN), false positive (FP), and false negative (FP) was created. The accuracy of the model was calculated as the fraction of pixels that correctly identified water and non-water areas, while precision denotes the fraction of pixels that correctly predicted water areas. The hit rate indicates how often the model successfully detects water, whereas the false alarm rate indicates how frequently the index mistook non-water as water. The miss rate is a measure of how often the model fails to recognize water, while the true negative rate shows how often the model correctly recognizes non-water (Magno *et al.* 2021).

The descriptive statistics for the water class are stated using the formula given in Equations (4)–(9) to reflect the outcome of the surface water detection and to evaluate the accuracy of the water delineation map:

$$\text{Accuracy} = \frac{\text{TP} + \text{TN}}{\text{Total number of pixels}} \times 100 \tag{4}$$

$$\text{Precision} = \frac{\text{TP}}{\text{TP} + \text{FP}} \times 100 \tag{5}$$

$$\text{Hit rate} = \frac{\text{TP}}{\text{TP} + \text{FN}} \times 100 \tag{6}$$

$$\text{False alarm rate} = \frac{\text{FP}}{\text{TP} + \text{FP}} \times 100 \tag{7}$$

$$\text{Miss rate} = \frac{\text{FN}}{\text{FN} + \text{TP}} \times 100 \tag{8}$$

$$\text{True negative rate} = \frac{\text{FN}}{\text{FN} + \text{TP}} \times 100 \tag{9}$$

3. RESULTS

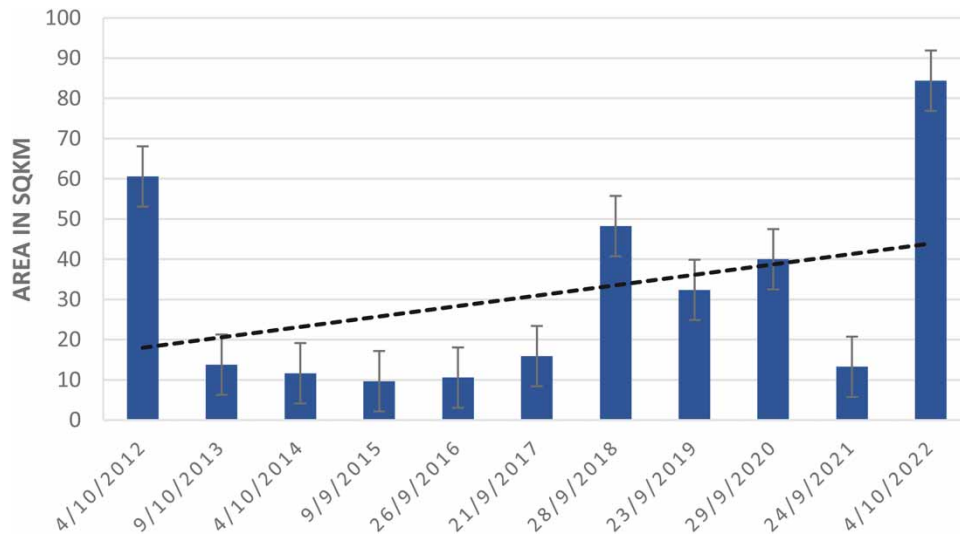### 3.1 Flood inundation extent from 2012 to 2020

Flood inundation in the confluence region of Rivers Niger and Benue was mapped using images from different sensors. The flood water derived during peak flooding in late September and early October from 2012 to 2022 is depicted in Figure 4(a)–4(k). It can be seen that the flood extent decreased from 2012 to 2015 but increased from 2016 to 2018. However, in 2019, the flood extent decreased, while an increase in the flood extent was observed in 2020. In 2021, the flood extent decreased, while in 2022, the extent of the flood increased remarkably (Figure 5).

On 4 October 2012, the flood extent was 60.57 km^2 (25.5%). The flood extent was 13.78 km^2 (5.8%) on 9 October 2013, 11.65 km^2 (4.9%) on 4 October 2014, and 10.56 km^2 (4.4%) on 9 September 2015. The values of the flood extent on 26 September 2016 and 21 September 2017 were 9.67 km^2 (4.0%) and 15.9 km^2 (6.7%), respectively. The areal extent of the flood on 28 September 2018 was 48.24 km^2 (20.4%), while the inundation extent on 23 September 2019 was 32.36 km^2 (13.65%). About 39.98 km^2 (16.9%) of the study area was inundated on 29 September 2020. The values of the flood extent on 24 September 2021 and 4 October 2022 were 13.25 km^2 (5.5%) and 84.29 km^2 (35.6%), respectively. Figure 6 shows the Sentinel-2 images before the flood on 20 September 2022 and during the flood on 4 October 2022.
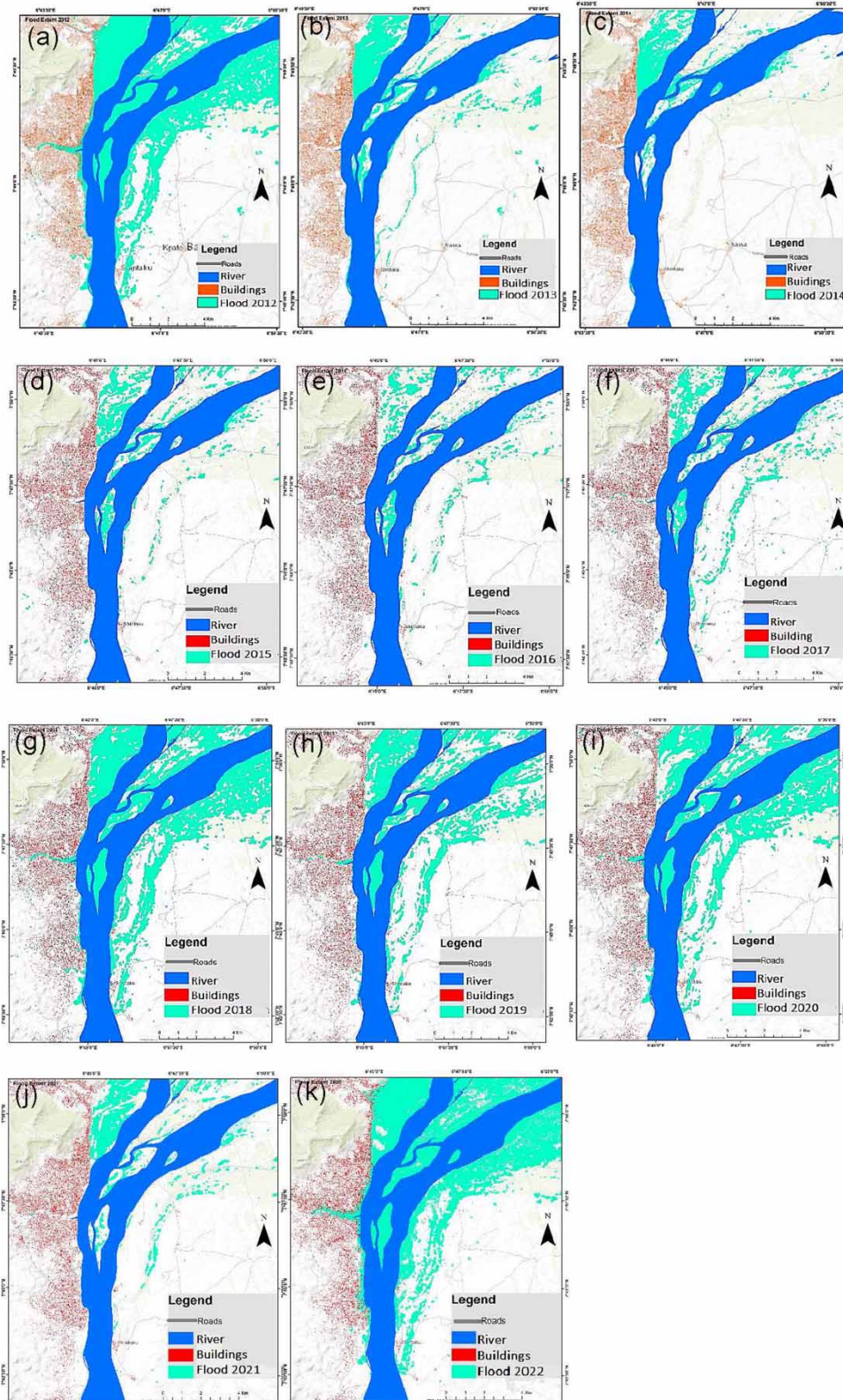
Figure 4 | Flood inundation for (a) 4 October 2012, (b) 9 September 2013, (c) 4 October 2014, (d) 20 September 2015, (e) 26 September 2016, (f) 21 September 2017, (g) 28 September 2018, (h) 23 September 2019, (i) 29 September 2020, (j) 24 September 2021, and (k) 4 October 2022.

Figure 5 | Flood inundation extent from 2012 to 2022.

The Sentinel-2 images and photographs were used to validate and geolocate the flood extent derived from the 4 October 2022 SAR image (Figure 7).

3.2. Performance evaluation of different sensors in water body extraction

For the performance among the three sensors and algorithms, Landsat-7 and Sentinel-2 performed much better than Landsat-8 in the extraction of water bodies. The overall accuracy for Landsat-7 was 91%, while Sentinel-2 was 96%. The improved accuracy of Sentinel-2 could be attributed to finer spatial resolution and marginal cloud cover. Landsat-8 achieved an accuracy of 88%, and cloud cover may have influenced the accuracy of the water extraction. The high hit rate and low miss rate for Landsat-7 and Sentinel-2 indicate the viability of the algorithms in discriminating water and non-water areas (Table 2).

3.3. Inundation frequency

The flood inundation frequency map for 10 years in the confluence region of Rivers Niger and Benue is shown in Figure 8. Areas with high flood frequency are represented in dark shadings. These areas are regularly inundated and found predominately in the floodplains in the northwestern part of the study area, where the flood frequency exceeded nine times. It was observed that buildings, population, roads, and cropland are near the areas of high inundation frequency. In the eastern part, the frequency of flood inundation is low, where the frequency was <4 times.

3.4. Damage assessment

3.4.1. Impacts on cropland

Croplands constitute 32.5% Land use/Land cover (LU/LC) of the confluence region. The decade of flooding has resulted in cumulative inundation of agricultural land estimated at 14,302 ha. The study area is prominent for maize production in the plain by small-scale farmers. The state is among the top 10 producers of maize in Nigeria. Data from the National Bureau of Statistics (2019) and PricewaterhouseCoopers (2021) analysis put Kogi's state total maize production in 2019 at 261,000 metric tons harvested from over 32,031,825 ha of land. The intensity of floods in the region during harvest time (usually September and October) inundated hundreds and thousands of cropland, especially maize farms. In 2012, the flooded cropland area was 1,912 ha, with estimated crop damage of 176,515 US dollars. For 2013 and 2014 flood events, the total inundated cropland areas were 1,150 and 818 ha, resulting in an estimated crop damage worth 114,264 and 90,781 US dollars, respectively. In the 2015 flood incident, about 632 ha of cropland was submerged, destroying maize farms of 81,553 US dollars. For 2016, the flooded cropland areas were 412 ha, with an estimated crop damage of 69,108 US dollars. The 2016 flood event was the lowest in terms of extent and damages. However, in 2017, the flood overran 890 ha of cropland, resulting in an estimated 183,749 US dollars worth of crop damage. The inundation extent of cropland was extensive in 2018, resulting in 1894 ha of cropland submerged and an estimated damage of 464,370 US dollars. The 2019 flood

Figure 6 | RGB true color display of Sentinel-2 before the flood on 20 September 2022 (a, c) and during the flood on 4 October 2022 (b, d).

inundated 1,579 ha of cropland, resulting in damages estimated at 411,582 US dollars. The total flooded cropland for 2020 and 2021 flood incidents was 1,790 and 1,286 ha, costing 923,926 and 696,960 US dollars worth of crop damages. The 2022 flood was considered the most severe event, with a total flooded cropland area of 2,227 ha and an estimated 1,264,401 US dollars worth of crop damages (Figure 9(a)–9(k) and Table 3). Figure 10 shows the photographs of inundated maize/rice fields captured on 6 October 2022.

3.4.2. Impact on household

The annual flooding in the region inundated households and displaced thousands of inhabitants. Figure 11(a)–11(k) shows the affected households from 2012to 2022. The number of buildings submerged in 2012 was 2,890, resulting in a temporary displacement of 11,527 persons, compared to the reference displacement of 10,000 persons reported by the National Emergency Management Agency (2016). In 2013, the number of affected buildings was 158 and the number of displaced inhabitants was 3,669. In 2014 and 2015, 89 and 189 buildings were submerged, displacing 1,372 and 1,241 inhabitants, respectively. In 2016, 81 buildings were inundated and 958 inhabitants had to temporarily leave their homes. In 2017, the number of affected buildings was 514 and 3,350 inhabitants were displaced. In 2018, a total of 1,018 buildings were affected and 9,529 inhabitants were displaced. The 2019 flood event submerged 267 buildings and temporarily displaced 6,461 inhabitants. The 2020 and 2021 flood incidents affected 713 and 56 buildings and displaced 8,565 and 1,170 inhabitants temporarily
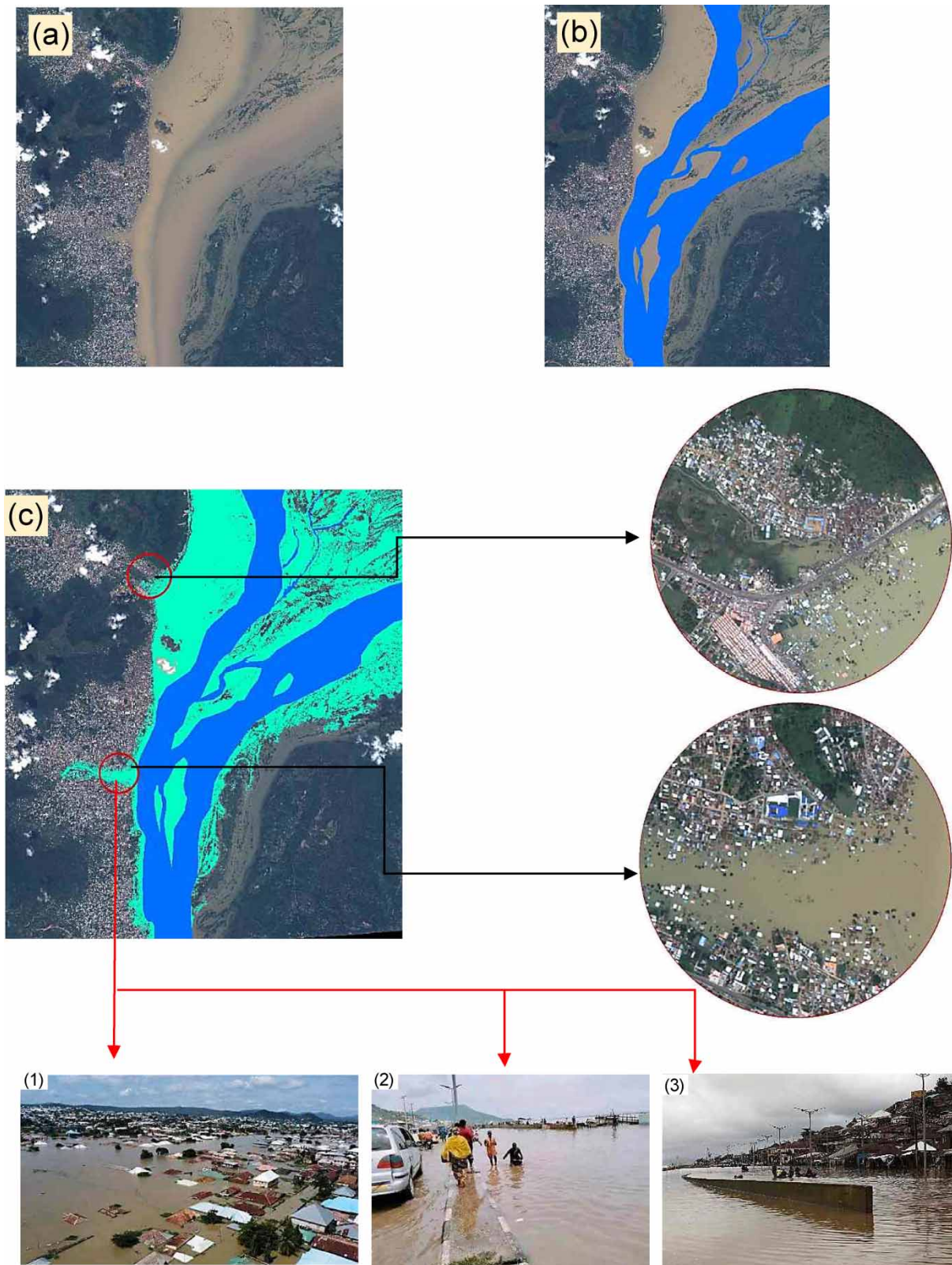
Figure 7 | Flood validation: (a) Sentinel-2 image of the flooded area on 4 October 2022, (b) overlay of permanent waterbodies to illustrate the flooded extent with the Sentinel-2 image in the background, and (c) overlay of the flooded area with the Sentinel-2 image, with black arrow pointing to the locations and red arrows indicating locations geolocated with field photographs in the plate: 1–3.

**Table 2** | Summary of performance of Sentinel-2, Landsat-7, and Landsat-8

Sensor	TP	FN	TN	FP	Accuracy	Precision	Hit rate	False alarm rate	Miss rate	True negative value
Landsat-7	48	11	32	9	91	84.21	81.36	15.79	18.64	78.05
Landsat -8	40	16	31	13	88	75.47	71.43	24.53	28.57	70.45
Sentinel-2	57	6	33	4	96	93.44	90.48	6.56	9.52	89.19
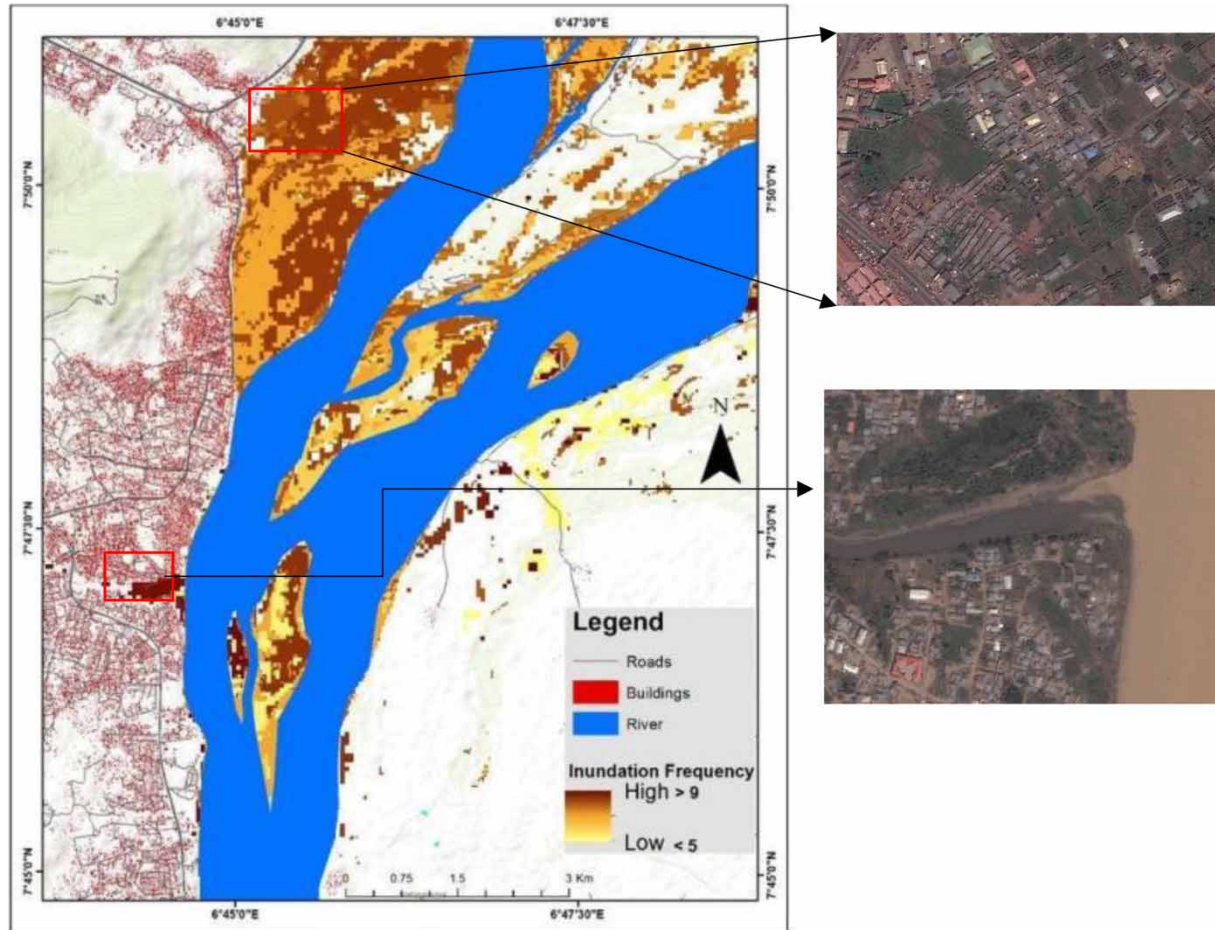
Figure 8 | Flood inundation frequency from 2012 to 2022. Inset: proximity of buildings and population.

from their houses, respectively. The 2022 incident affected 6,941 buildings and displaced 36,390 inhabitants, compared to 2,600 inhabitants reported by the International Organisation for Migration (IOM) (2022) (Table 4 and Figure 13).

3.4.3. Impact on population

Thousands of individuals have been affected by flooding in the region from 2012 to 2022, as shown in Figure 12(a)–12(k). On 4 October 2012, over 11,527 individuals were affected, while 3,669 individuals were affected on 9 October 2013. The estimated numbers of individuals affected on 4 October 2014 and 9 September 2015 were 1,372 and 1,241, respectively. On 26 September 2016 and 21 September 2017, the estimated numbers of individuals affected were 958 and 3,350, respectively. The number of individuals affected increased to 9,529 on 28 September 2018, while 6,461 individuals were affected on 23 September 2019. On 29 September 2020, an estimated 8,565 individuals were affected, and on 24 September 2021, a total of 1,170 individuals were affected. The highest number of individuals affected was estimated at 36,390 on 4 October 2022 (Table 4 and Figure 13).
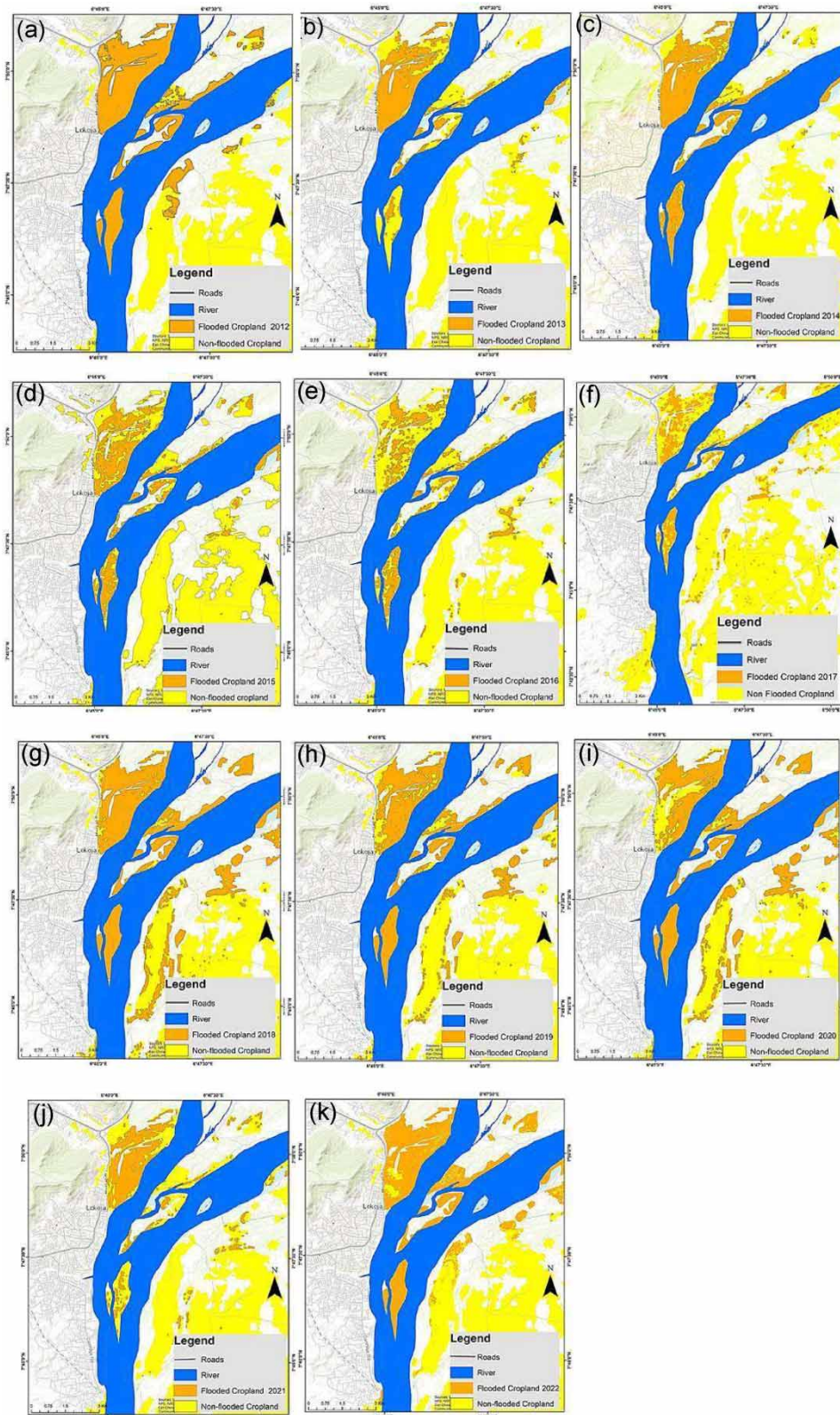
Figure 9 | Cropland inundated: (a) 4 October 2012, (b) 9 September 2013, (c) 4 October 2014, (d) 20 September 2015, (e) 26 September 2016, (f) 21 September 2017, (g) 28 September 2018, (h) 23 September 2019, (i) 29 September 2020, (j) 24 September 2021, and (k) 4 October 2022.

Table 3 | Estimated damages to crop

| Year	Inundated cropland (ha)	% inundated cropland	Average yield/tons/per ha	Cost per metric ton ($)	Estimated cost of maize damage ($)
2012	1,912	24.8	2	46.16	176,515.84
2013	1,150	14.9	2	49.68	114,264.00
2014	818	10.6	2	55.49	90,781.64
2015	632	8.2	2	64.52	81,553.28
2016	412	5.3	2	83.87	69,108.88
2017	890	11.9	2	103.23	183,749.40
2018	1,894	24.5	2	122.59	464,370.92
2019	1,579	20.5	2	130.33	411,582.14
2020	1,790	23.2	2	258.08	923,926.40
2021	1,286	16.7	2	270.98	696,960.56
2022	2,227	28.9	2	283.88	1,264,401.52
Total	14,590				4,477,214.58

Figure 10 | Affected maize/rice fields on 6 October 2022.

4. DISCUSSION

The confluence region of Rivers Niger and Benue is located in one of the most susceptible flood zones in Nigeria due largely to the floodplain. The peak flood period in the study area is between late September and early October. Other factors that amplify the vulnerability of this region to flooding include severe rainstorms and the occasional release of water from the Lagdo Dam in Cameroon. Multi-sensor satellite images were used to map the trajectory of flood inundation in the confluence region from 2012 to 2022. The findings revealed that within the decade, significant flooding incidents with profound damages were observed in 2012, 2018, 2020, and 2022.

In 2012, heavy rainfall resulted in an increase in water level in the Lagdo Dam on the River Benue channel and the Kainji Dam on the River Niger channel (Emmanuel & Eyoh 2017). When the floodgates of the dams were opened, a large volume of water was discharged, cascading downstream and resulting in the inundation of towns, communities, and cropland along the channel. Consequently, over 11,527 individuals were directly affected, with over 2,890 buildings either partly or fully submerged and over 1,912 ha of cropland affected. Hundreds of kilometers of roads were overrun, impeding motorists' access to the county's capital and other parts of the country. Across Nigeria, the 2012 flood affected 32 out of 36 states, with more than 7.7 million people affected and 363 deaths. More than 387,153 persons were displaced, 597,476 houses were damaged, and 14,500 km^2 (1.6% of the total area) was flooded (OCHA 2012).

The 2018 flood incident was the consequence of intense rainfall, which ravaged 48.24 km^2 (20.4%) of the study area. The scale of inundation was similar to the study conducted by Jimoh & Salami (2020). The 2018 flood submerged 18.9 km^2 of
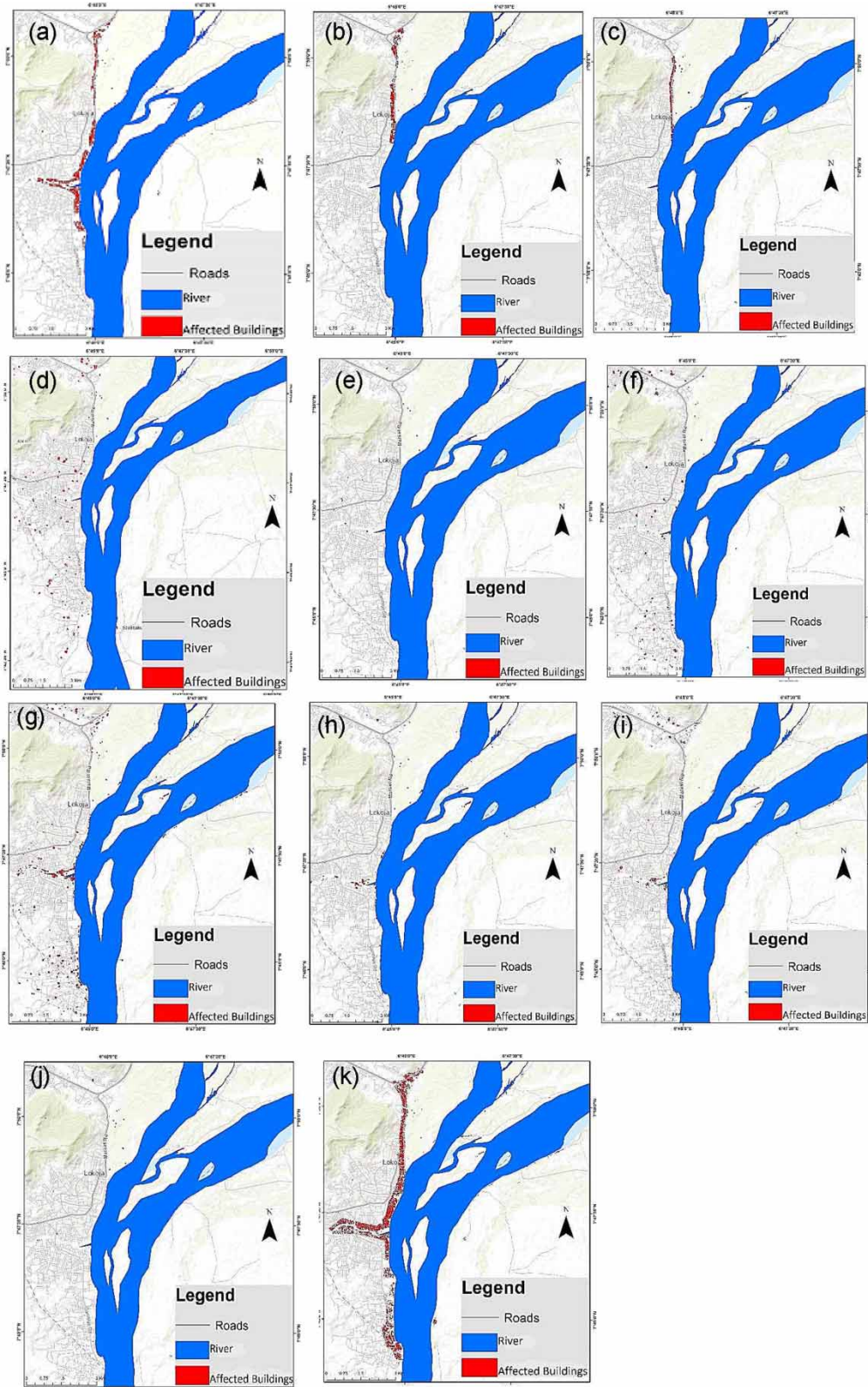
Figure 11 | Affected buildings: (a) 4 October 2012, (b) 9 September 2013, (c) 4 October 2014, (d) 20 September 2015, (e) 26 September 2016, (f) 21 September 2017, (g) 28 September 2018, (h) 23 September 2019, (i) 29 September 2020, (j) 24 September 2021, and (k) 4 October 2022.

**Table 4** | Number of inundated buildings and affected population

Year	Number of inundated buildings	Population affected
2012	2,890	11,527
2013	158	3,669
2014	89	1,372
2015	189	1,241
2016	81	958
2017	514	3,350
2018	1,018	9,529
2019	267	6,461
2020	713	8,565
2021	56	1,170
2022	6,941	36,390

cropland, damaged 1,018 buildings, and affected 9,529 individuals. Torrential rains in many parts of Nigeria unleashed floods in 12 states, affecting 2,321,592 individuals and displacing 722,741 inhabitants. The floods destroyed shelters, caused significant losses to livelihoods and the local economy, and resulted in high rates of water-borne diseases among the affected population and their host communities. Internally displaced peons living in host communities were especially vulnerable to cholera and other water-borne diseases due to limited access to potable water, hygiene infrastructure, and medical care (Disaster 2018).

In 2020, the rivers overshot their banks after a massive rainstorm, submerging over 39.98 km^2 of the areas. Consequently, 713 buildings were inundated, 8,565 individuals were affected, and 1,790 ha of cropland damaged. Roads and highways were flooded, thereby affecting the movement of goods and services within and outside the city. In 2022, intense rainfall and the release of excess water from the Lagdo Dam in Cameroon were responsible for the widespread flooding along the River Benue channel. The surging water from the dam inundated about 84.39 km^2 of the area and 2,227 ha of cropland. About 36,390 individuals and 6,941 buildings were affected. The scale of devastation of the 2022 flood has been described as the worst in the decade and almost similar to that of the 2012 flood. Across the country, over 2.4 million individuals were displaced and more than 660 individuals died. The devastating floods rendered 174,000 houses unfit for human habitation and also damaged over 676,000 ha of farmland in some areas during the harvest season, potentially worsening the country's already alarming levels of hunger and malnutrition (OCHA 2022a). From an agricultural standpoint, over 4.47 million US dollars worth of maize could have been affected in 10 years. In 2012, 2018, 2020, and 2022, maize was disproportionately affected by floods, with losses estimated at 176,515, 464,370, 923,926, and 1.2 million US dollars. In fact, the floods have impacted maize production and raised the cost of grain (Metu et al. 2016; Durodola 2019; Week & Wizor 2020; Echendu 2022). According to the National Agricultural Extension Research and Liaison Services (NAERLS), the 2022 flood inundated 863,648 ha of farmland across the country, causing a total loss of 92.78 million US dollars. This includes the loss of 8.4 million tons of crop outputs worth 296.91 million US dollars (Duntoye et al. 2023).

Nigeria's climate is changing, as evidenced by rising temperatures, variable rainfall, and increased flooding. Large runoffs and flooding have occurred in many areas of Nigeria due to longer and more intense rainstorms. The variability of rainfall is anticipated to get worse. Some regions are predicted to experience more precipitation and flooding (Haider 2019). Flooding in the confluence region has become frequent and intense, especially in the last 5 years due to urbanization and climate change. This has gravely impacted the lives, livelihoods, and properties on the banks of the river. The financial implications are too much of a burden to bear by the inhabitants, who mostly are peasant farmers and petty traders, even as they anticipate the next flood occurrence. Effective flood mitigation is therefore imperative, given that the study area has seen a lot of devastation. Interestingly, efforts have been made by the government to construct dykes on the river banks, but they have been ineffectual.

The flood inundation mapping reveals the situation in the region, underscoring the need for mitigation strategies. Mapping flood inundation can assist policymakers and stakeholders in developing actionable policies for flood management frameworks.
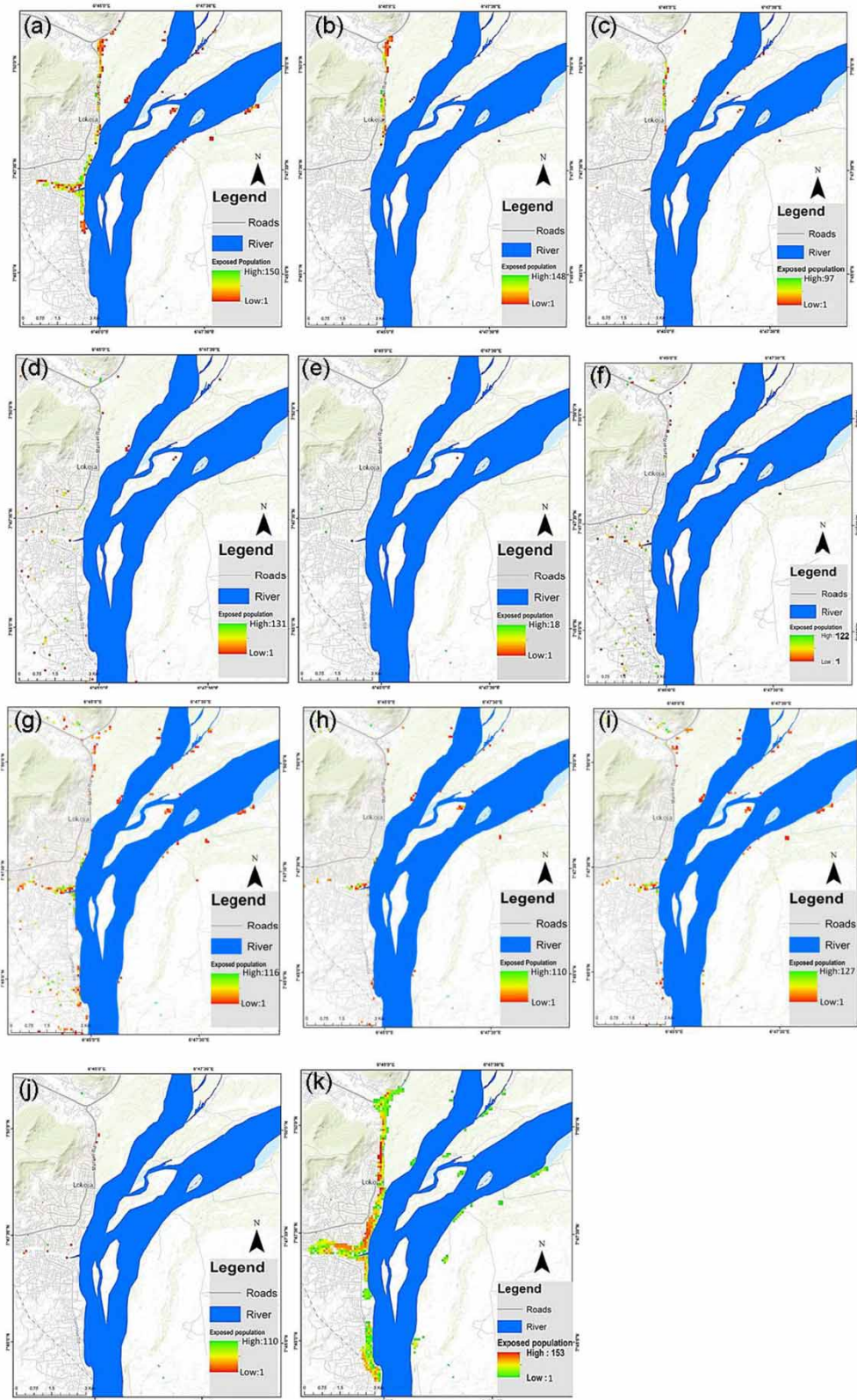
Figure 12 | Affected population: (a) 4 October 2012, (b) 9 September 2013, (c) 4 October 2014, (d) 20 September 2015, (e) 26 September 2016, (f) 21 September 2017, (g) 28 September 2018, (h) 23 September 2019, (i) 29 September 2020, (j) 24 September 2021, and (k) 4 October 2022.
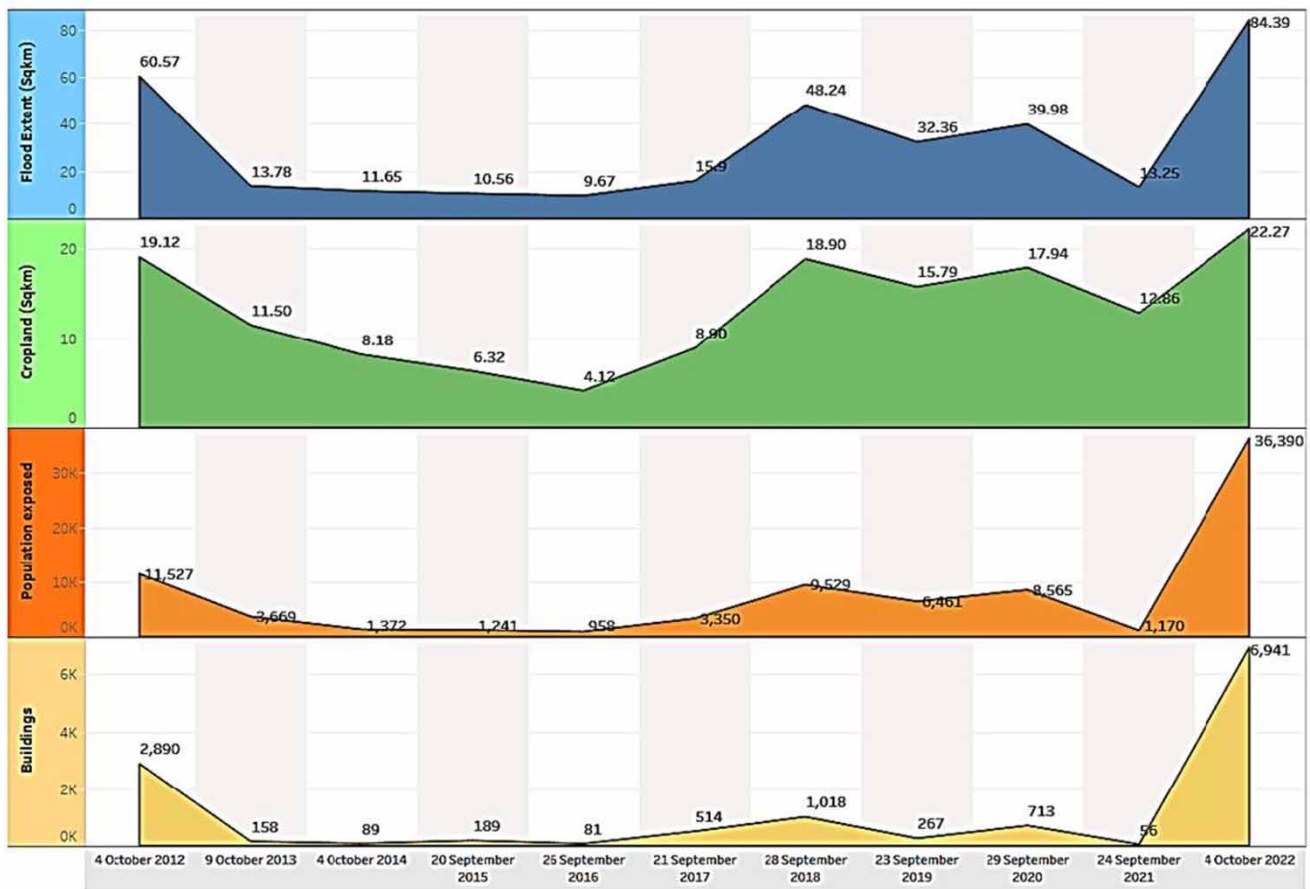
Figure 13 | Area chart for flood extent, cropland, population, and buildings.

5. CONCLUSION

This study mapped the decadal dynamics of flooding in the confluence region of Rivers Niger and Benue using multi-sensor data and GEE. The Sentinel-1 SAR data were processed to detect and extract surface water using the GEE interface. Additionally, NDWI and MNDWI were used to detect and extract surface water from Sentinel-2 datasets and Landsat-7 and Landsat-8 images.

The findings of the study revealed that within the decade, there had been four significant flooding incidents in 2012, 2018, 2020, and 2022, with inundation over 60.57, 48.24, 39.98, and 84.39 km^2, respectively. Damage assessment was done by intersecting flood extent on cropland, population, and building, and the analysis revealed that 12,916 buildings, 84,232 individuals, and 14,302 ha of cropland were adversely affected in the last 10 years. As a result, thousands of individuals have been displaced and forced to flee their ancestral homes, and crops of tens of millions of dollars have been damaged. The exploitation of multi-sensor images has proven to be indispensable for large-scale flood mapping. Flood impact assessment methods, as well as information on affected croplands and populations, can assist disaster managers and policymakers in taking flood mitigation measures and assessing flood risk in vulnerable populated areas.

AUTHOR CONTRIBUTIONS

CO conducted data acquisition, developed the methodology, and prepared the original draft. GJ supervised the manuscript. AO supervised and edited the manuscript. SK performed data cleaning and processing. BO and HI reviewed and visualized articles. OA and AT proofread the manuscript.

DATA AVAILABILITY STATEMENT

All relevant data are included in the paper or its Supplementary Information.

CONFLICT OF INTEREST

The authors declare there is no conflict.

REFERENCES

Acharya, T., Subedi, A. & Lee, D. 2018 Evaluation of water indices for surface water extraction in a Landsat 8 scene of Nepal. *Sensors* **18**, 2580. https://doi.org/10.3390/s18082580.

Adedeji, O., Olusola, A., Babamaaji, R. & Adelabu, S. 2021 An assessment of flood event along Lower Niger using Sentinel-1 imagery. *Environmental Monitoring and Assessment* **193** (12), 858. https://doi.org/10.1007/s10661-021-09647-1.

Aderoju, O., Jantiku, J., Fagbemiro, O., Aliyu, I., Nwadike, K., Ajonye, S. & Salman, K. 2014 Geospatial assessment of 2012 flood disaster in Kogi state, Nigeria. *IOSR Journal of Environmental Science, Toxicology and Food Technology (IOSR-JESTFT)* **8**. https://doi.org/10.9790/2402-08247484.

Anusha, N. & Bharathi, B. 2020 Flood detection and flood mapping using multi-temporal synthetic aperture radar and optical data. *Egyptian Journal of Remote Sensing and Space Science* **23** (2), 207–219. https://doi.org/10.1016/j.ejrs.2019.01.001.

Buma, W. G., Lee, S. I. & Seo, J. Y. 2018 Recent surface water extent of lake Chad from multispectral sensors and GRACE. *Sensors (Switzerland)* **18** (7). https://doi.org/10.3390/s18072082.

Centre for Research on the Epidemiology of Disasters. 2020 Human cost of disasters (2000–2019). *Human Cost of Disasters* **61**, 1–2. https://doi.org/10.1186/s12889.

Cohen, S., Raney, A., Munasinghe, D., Loftis, J. D., Molthan, A., Bell, J., Rogers, L., Galantowicz, J., Brakenridge, G. R. & Kettner, A. J. 2019 The Floodwater Depth Estimation Tool (FwDET v2. 0) for improved remote sensing analysis of coastal flooding. *Natural Hazards and Earth System Sciences* **19** (9), 2053–2065.

Diaz, J. H., Brisolara, K. F., Harrington, D. J., Hu, C.-Y. & Katner, A. L. 2020 The environmental health impact of Hurricane Katrina on New Orleans. *American Journal of Public Health* **110** (10), 1480–1484. https://doi.org/10.2105/AJPH.2020.305809.

Dinh, D. A., Elmahrad, B., Leinenkugel, P. & Newton, A. 2019 Time series of flood mapping in the Mekong Delta using high resolution satellite images. *IOP Conference Series: Earth and Environmental Science* **266** (1). https://doi.org/10.1088/1755-1315/266/1/012011.

Disaster, N. 2018 *National Emergency Management Agency 2018 Floods – Situation Report No 1 (21 September 2018)*. pp. 2–4.

Duntoye, S. & Saad, U. & NCAT. 2023 *Smallholder Farmer Practices to Counter Flooding and Drought in Northeast Nigeria* USAID, Washington, DC.

Durodola, O. S. 2019 The impact of climate change induced extreme events on agriculture and food security: A review on Nigeria. *Agricultural Sciences* **10** (4), 487–498.

Ebinne, E. & Apeh, O. I. 2019 Satellite-based flood mapping for impact assessments: a case study in Lokoja, Kogi State, Nigeria. *International Journal of Advances in Science, Engineering and Technology* **7** (2), 5–8.

Echendu, A. J. 2022 Flooding, food security and the sustainable development goals in Nigeria: Assemblage and systems thinking approach. *Social Sciences* **11** (2). https://doi.org/10.3390/socsci11020059.

Emmanuel, A. & Eyoh, A. (2017). *Section A: Environmental Science Spatial Analysis of River Inundation and Flood Risk Potential along Kogi State River Niger-Benue Basin Using Geospatial Techniques*. 666, pp. 351–364. E-ISSN: 2278–179X. Available from: www.jecet.org.

Güvel, Ş. P., Akgül, M. A. & Aksu, H. 2022 Flood inundation maps using Sentinel-2: A case study in Berdan Plain. *Water Supply* **22** (4), 4098–4108.

Haider, H. 2019 *Climate Change in Nigeria: Impacts and Responses. K4D Helpdesk Report*, pp. 1–38. Available from: http://www.rockfound.org/initiatives/climate/climate_change.shtml%0Awww.iied.org/HS/publications.html.%0AHOW%0Ahttps://assets.publishing.service.gov.uk/media/5dcd7a1aed915d0719bf4542/675_Climate_Change_in_Nigeria.pdf.

Huang, C., Chen, Y. & Wu, J. 2014 Mapping spatio-temporal flood inundation dynamics at large riverbasin scale using time-series flow data and MODIS imagery. *International Journal of Applied Earth Observation and Geoinformation* **26** (1), 350–362. https://doi.org/10.1016/j.jag.2013.09.002.

International Institute of Tropical Agriculture IITA. 2011 *IITA Annual Report 2011*. IITA, Ibadan, Nigeria. Available from: https://www.iita.org/wp-content/uploads/2016/04/Annual-Report-2011.pdf.

International Organisation for Migration (IOM). 2022 *Flood Rapid Needs Assessment – Kogi State. IOM UN Migration – Nigeria, 2022 (October)*, pp. 1–5. Available from: https://dtm.iom.int/nigeria (accessed 15 November 2022).

Ji, L., Zhang, L. & Wylie, B. 2009 Analysis of dynamic thresholds for the normalized difference water index. *Photogrammetric Engineering & Remote Sensing* **75** (11), 1307–1317.

Jimoh, U. U. & Salami, H. 2020 Spatio-temporal analysis of flooding in Lokoja (1999-2018), Kogi State Nigeria. *International Journal of Scientific Research in Multidisciplinary Studies* **6** (2), 58–72.

Khan, S. I., Adhikari, P., Hong, Y., Vergara, H., Adler, R. F., Policelli, F., Irwin, D., Korme, T. & Okello, L. 2011 Hydroclimatology of Lake Victoria region using hydrologic model and satellite remote sensing data. *Hydrology and Earth System Sciences* **15** (1), 107–117.

Kuldeep, Garg, P. K. & Garg, R. D. 2016 Geospatial techniques for flood inundation mapping. In *International Geoscience and Remote Sensing Symposium (IGARSS),* Beijing, China, 10–15 July 2016. IEEE, New York, pp. 4387–4390. https://doi.org/10.1109/IGARSS.2016.7730143.

Kumar, L. & Mutanga, O. 2018 Google earth engine applications since inception: Usage, trends, and potential. *Remote Sensing* **10** (10), 1509.

Kumar, H., Karwariya, S. K. & Kumar, R. 2022 Google Earth Engine-based identification of flood extent and flood-affected paddy rice fields using Sentinel-2 MSI and Sentinel-1 SAR data in Bihar State, India. *Journal of the Indian Society of Remote Sensing* **50** (5), 791–803. https://doi.org/10.1007/s12524-021-01487-3.

Magno, R., Rocchi, L., Dainelli, R., Matese, A., Di Gennaro, S., Chen, C.-F., Thanh Son, N. & Toscano, P. 2021 Agroshadow: A new Sentinel-2 cloud shadow detection tool for precision agriculture. *Remote Sensing* **13**, 1219. https://doi.org/10.3390/rs13061219.

Metu, A. G., Okeyika, K. O. & Maduka, O. D. 2016 Achieving sustainable food security in Nigeria: Challenges and way forward. In *3rd International Conference on African Development Issues (CU-ICADI)*, pp. 182–187.

Mondejar, J. P. & Tongco, A. F. 2019 Near infrared band of Landsat 8 as water index: A case study around Cordova and Lapu-Lapu City, Cebu, Philippines. *Sustainable Environment Research* **29** (1), 16. https://doi.org/10.1186/s42834-019-0016-5.

National Bureau of Statistics. 2019 *(Q1 2019) Report Date: May 2019 Methodology*. May. Available from: https://nigerianstat.gov.ng/download/937.

National Emergency Management Agency. 2016 *NEMA Situation Report. 6(August)*, p. 128.

Nghia, B. P. Q., Pal, I., Chollacoop, N. & Mukhopadhyay, A. 2022 Applying Google Earth Engine for flood mapping and monitoring in the downstream provinces of Mekong river. *Progress in Disaster Science* **14**, 100235. https://doi.org/10.1016/j.pdisas.2022.100235.

Nigeria Commodity Exchange. 2021 Nigeria Commodity Exchange Notes. November. Available from: https://nigeriacommex.com/ncx-notes/67-nigeria-commodity-exchange-notes.html.

OCHA. 2012 *Country Emergency Situation Report No. 1/2. 2(2)*, pp. 21–23. Available from: www.unocha.org.

OCHA. 2022a *Situation Report – Nigeria. Last Updated: 1 Nov 2022*. pp. 1–25. Available from: https://reports.unocha.org/en/country/nigeria/.

OCHA. 2022b *West and Central Africa Flooding Situation – Overview*. December, pp. 1–3.

Otsu, N. 1979 A threshold selection method from gray-level histograms. *IEEE Transactions on Systems, Man, and Cybernetics* **9** (1), 62–66.

Pandey, A. C., Kaushik, K. & Parida, B. R. 2022 Google Earth Engine for large-scale flood mapping using SAR data and impact assessment on agriculture and population of Ganga-Brahmaputra Basin. *Sustainability (Switzerland)* **14** (7). https://doi.org/10.3390/su14074210.

Pekel, J.-F., Cottam, A., Gorelick, N. & Belward, A. 2016 High-resolution mapping of global surface water and its long-term changes. *Nature* **540**. https://doi.org/10.1038/nature20584.

Phy, S. R., Sok, T., Try, S., Chan, R., Uk, S., Hen, C. & Oeurng, C. 2022 Flood hazard and management in Cambodia: a review of activities, knowledge gaps, and research direction. *Climate* **10** (11), 162. https://doi.org/10.3390/cli10110162.

PricewaterhouseCoopers. 2021 *Africa's Leader in Maize* (Issue September). Available from: https://www.pwc.com/ng/en/assets/pdf/positioning-nigeria-as-africa-leader-in-maize-production-for-afcfta.pdf.

Rangari, V. A., Umamahesh, N. V. & Bhatt, C. M. 2019 Assessment of inundation risk in urban floods using HEC RAS 2D. *Modeling Earth Systems and Environment* **5** (4), 1839–1851. https://doi.org/10.1007/s40808-019-00641-8.

Rentschler, J. & Salhab, M. 2020 People in Harm's Way: Flood Exposure and Poverty in 189 Countries. *Policy Research Working, October*, Policy Working Paper 9447. Available from: https://openknowledge.worldbank.org/handle/10986/34655.

Risling, A. 2022 *Evaluation of a Change Detection Approach to Map Global Flood Extents Using Sentinel-1*. Available from: https://kth.diva-portal.org/smash/get/diva2:1677122/FULLTEXT01.pdf.

Sahoo, S. N. & Sreeja, P. 2017 Development of flood inundation maps and quantification of flood risk in an urban catchment of Brahmaputra river. *ASCE-ASME Journal of Risk and Uncertainty in Engineering Systems, Part A: Civil Engineering* **3** (1). https://doi.org/10.1061/ajrua6.0000822.

Suab, S. A., Supe, H., Avtar, R., Dambul, R. & Chen, X. 2022 Detection and mapping of May 2021 flood in Beaufort, Sabah using Sentinel-1 SAR and Sentinel-2 multispectral in Google Earth Engine. In *IOP Conference Series: Earth and Environmental Science, 1064(1)*. https://doi.org/10.1088/1755-1315/1064/1/012003.

Suhr, F. & Steinert, J. I. 2022 Epidemiology of floods in sub-Saharan Africa: a systematic review of health outcomes. *BMC Public Health* **22** (1), 268. https://doi.org/10.1186/s12889-022-12584-4.

Thito, K., Wolski, P. & Murray-Hudson, M. 2016 Mapping inundation extent, frequency and duration in the Okavango Delta from 2001 to 2012. *African Journal of Aquatic Science* **41** (3), 267–277. https://doi.org/10.2989/16085914.2016.1173009.

Tiwari, V., Kumar, V., Matin, M. A., Thapa, A., Ellenburg, W. L., Gupta, N. & Thapa, S. 2020 Flood inundation mapping – Kerala 2018; harnessing the power of SAR, automatic threshold detection method and Google Earth Engine. *PLoS One* **15**, 1–17. https://doi.org/10.1371/journal.pone.0237324.

Tripathy, P. & Malladi, T. 2022 Global flood mapper: A novel Google Earth Engine application for rapid flood mapping using Sentinel-1 SAR. *Natural Hazards* **114** (2), 1341–1363. https://doi.org/10.1007/s11069-022-05428-2.

United Nations Disaster Risk Reduction Preparedness, & Asian Disaster Preparedness Center. 2019 *Disaster Risk Reduction in Cambodia Status Report*. pp. 1–32. Available from: https://reliefweb.int/sites/reliefweb.int/files/resources/68230_1cambodiaupdaed16oct2019.pdf.

Vanama, V. S. K., Mandal, D. & Rao, Y. S. 2020 GEE4FLOOD: Rapid mapping of flood areas using temporal Sentinel-1 SAR images with Google Earth Engine cloud platform. *Journal of Applied Remote Sensing* **14** (03), 1. https://doi.org/10.1117/1.jrs.14.034505.

Vekaria, D., Chander, S., Singh, R. P. & Dixit, S. 2022 A change detection approach to flood inundation mapping using multi-temporal Sentinel-1 SAR images, the Brahmaputra River, Assam (India): 2015–2020. *Journal of Earth System Science* **132** (1), 3. https://doi.org/10.1007/s12040-022-02020-x.

Wang, Q., Zhuo, L., Rico-ramirez, M., Han, D., Wang, J., Liu, Y. & Du, S. 2022a *Flood Inundation Mapping Using Sentinel-1 SAR Images with Google Earth Engine Cloud Platform*. EGU General Assembly 2022, Vienna, Austria, 23–27 May 2022. Available from: https://doi.org/10.5194/egusphere-egu22-5877.

Week, D. A. & Wizor, C. H. 2020 Effects of flood on food security, livelihood and socio-economic characteristics in the flood-prone areas of the core Niger Delta, Nigeria. *Asian Journal of Geographical Research* **3** (1), 1–17.

World Meteorological Organization. 2022 *Assessment Guidelines for End-to-End Flood Forecasting and Early Warning Systems 2022* (Issue 1286). Available from: https://library.wmo.int/doc_num.php?explnum_id=11379.

Xu, H. 2006 Modification of normalised difference water index (NDWI) to enhance open water features in remotely sensed imagery. *International Journal of Remote Sensing* **27** (14), 3025–3033.

Zhou, Y., Dong, J., Xiao, X., Xiao, T., Yang, Z., Zhao, G., Zou, Z. & Qin, Y. 2017 Open surface water mapping algorithms: A comparison of water-related spectral indices and sensors. *Water* **9**, 256. https://doi.org/10.3390/w9040256.